Comparison of methods for detection and characterization of exoplanets with SPHERE/IRDIS

A. Vigan[a], C. Moutou[a], M. Langlois[b], D. Mouillet[c], K. Dohlen[a], A. Boccaletti[d], M. Carbillet[e], I. Smith[e], A. Ferrari[e], L. Mugnier[f] and C. Thalmann[g]

[a] LAM, UMR 6110, CNRS, Université de Provence, 38 rue Frédéric Joliot-Curie, 13388 Marseille Cedex 13, France;
[b] CRAL, UMR 5574, CNRS, Université Claude Bernard, 9 avenue Charles André, 69561 Saint Genis Laval Cedex, France;
[c] LAOG, UMR 5571, CNRS, Université Joseph-Fourier, BP 53, 38041 Grenoble Cedex 9, France;
[d] LESIA, UMR 8109, Observatoire de Paris, CNRS, Université Paris-Diderot, 5 place Jules Janssen, 92195 Meudon Cedex, France;
[e] Laboratoire Fizeau, UMR 6525, Université de Nice Sophia Antipolis, Observatoire de la Côte d'Azur, CNRS, Parc Valrose, 06108 Nice Cedex 2, France;
[f] ONERA, DOTA, BP 72, 92322 Chatillon Cedex, France;
[g] MPIA, Königstuhl 17, 69117 Heidelberg, Germany;

ABSTRACT

SPHERE is a second generation instrument for the Very Large Telescope (VLT) which will aim at directly detecting the intrinsic flux of young giant exoplanets thanks to a dedicated extreme adaptive optics system and coronagraphs. Exoplanet detection in the near-infrared will be performed in parallel with an integral field spectrograph and a differential imager, IRDIS. IRDIS main mode for exoplanet detection will be Dual-Band Imaging (DBI) where two images are acquired simultaneously at close wavelengths around expected sharp features in cold planetary objects spectra. We present here the end-to-end simulations performed to obtain realistic data for IRDIS in DBI mode with temporal evolution of the quasi-static speckle pattern. Data cubes have been generated to represent 4 hour observations in IRDIS filter pairs for various star magnitudes and planets at angular separations from $0''.2$ to $2''.0$. Using this unique set of data, we present a comparison of various data analysis methods for high-contrast imaging with IRDIS in DBI mode both in terms of detection limits and of estimation of the exoplanet flux after speckle noise attenuation.

Keywords: High angular resolution; High contrast; Data analysis; Instrument: VLT-SPHERE, IRDIS

1. INTRODUCTION

Most of the exoplanets currently known have been detected with indirect methods such as radial velocities or transits. Although these methods are mainly sensitive to planets at small orbital separations ($\lesssim$ 5 AU), some stars are showing long term trends that may indicate the presence of distant planetary companions. The wide use of adaptive optics systems on large ground-based telescopes has recently allowed to start probing for low mass companions at large orbital distances from nearby stars, leading to the image of the first exoplanet in 2005 around the young brown dwarf 2MASSW-J1207334-393254. In the following years, a handful of these objects have been imaged with existing instruments, such as DH Tau B, GQ Lup b, AB Pic b, CHXR 73 B, and more recently Fomalhaut b, 1RXS J1609 b, β Pic b, the triple system around HR 8799, and GJ 758 B.

SPHERE (Spectro-Polarimetric High-conrast Exoplanet REsearch) is a second generation instrument for the VLT (Very Large Telescope) at ESO-Paranal Observatory which will be dedicated to the direct detection of

Send correspondence to A. Vigan:
E-mail: arthur.vigan@oamp.fr
Telephone: +33.4.95.04.41.49

Ground-based and Airborne Instrumentation for Astronomy III, edited by Ian S. McLean, Suzanne K. Ramsay, Hideki Takami, Proc. of SPIE Vol. 7735, 77352X · © 2010 SPIE · CCC code: 0277-786X/10/$18 · doi: 10.1117/12.856701

Downloaded From: http://proceedings.spiedigitallibrary.org/ on 11/30/2016 Terms of Use: http://spiedigitallibrary.org/ss/termsofuse.aspx

exoplanets and low mass companions around nearby stars. Similar instruments are currently being built for other telescopes, such as GPI[1] (Gemini Planet Imager) for Gemini South and HiCIAO[2] (High-contrast Coronagraphic Imager for Adaptive Optics) for Subaru. This next generation of instruments aims at detecting young exoplanets down to the Jupiter mass (M_{Jup}) by reaching contrast values of 10^{-6} to 10^{-7} at angular separations as small as $\sim 0''.1$. In order to achieve such high performances, SPHERE will use an extreme adaptive optics system[3] of 40×40 actuators to reach very high corrections in the near-infrared ($\sim$90% Strehl in H band), and high efficiency coronagraphs to obtain optimal star extinction. Different types of coronagraphs will be available such as the achromatic 4-quadrant phase mask[4,5] or the apodized pupil Lyot coronagraph.[6] SPHERE will have two scientific instruments working in the near-infrared: a diffraction-limited integral field spectrograph[7] (IFS), and a differential spectro-imager[8] (IRDIS). IRDIS will support several observing modes including Dual-Band Imaging (DBI) which will provide simultaneous images at two close wavelengths in one of its 5 different filter pairs covering Y to Ks bands. The IFS will be diffraction-limited in the near-infrared and will provide spectra from Y to H bands.

In this work, we present the end-to-end simulations that we have performed in order to obtain a realistic 4-hours sequence of observation with IRDIS in DBI mode with 4 different filter pairs, and the results obtained in terms of exoplanet detection and intrinsic flux estimation. In Sect. 2 we present the parameters of our simulations. In Sect. 3, after reminding the intrinsic limitations of high-contrast imaging, we present the detection performances with data analysis methods developed in the context of direct imaging: SDI (Spectral Differential Imaging), ADI (Angular Differential Imaging), LOCI (Locally Optimized Combination of Images) and their possible combinations. Finally in Sect. 4 we present the results in terms of planet flux estimation as a function of contrast estimated on data analyzed with ADI, SDI+ADI and MOODS (MOving Object Detection for Sphere), a data analysis method developed in the context of SPHERE.

2. END-TO-END SIMULATIONS

An end-to-end model of the SPHERE instrument has been developed to test the performances of the different modes of the instrument. It is a diffractive code written in IDL* based on the CAOS (Code for Adaptive Optics Systems) problem solving environment[9] with a specific package developed for the SPHERE project.[10]

This model includes a large number of effects at different spatial and temporal scales. It has been used to simulate a realistic test case for SPHERE, which is the observation of a star at a declination $\delta = -45°$ covering hour angles of -2 hr to +2 hr with an apodized pupil Lyot coronagraph. The following effects have been accounted for:

- AO correction of the turbulent wavefront: for each image, 100 decorrelated phase screens have been used to simulate the AO-corrected atmosphere,
- Variation of the seeing and wind speed with time, and thus of the quality of the AO correction,
- Image formation down to the detector taking into account the different optical elements and instrumental effects (coronagraph, chromaticism, DBI filters, ...),
- Effects related to the changing airmass and field rotation: ADC chromatic residuals, optics rotation (entrance window, derotator, ADC, beam shift),
- Variations on long timescales: temperature, pointing stability, pupil translation, rotation residuals, focusing on the coronagraph,
- Detector effects: photon noise, RON, flat field noise
- Photometry: global instrumental throughput, realistic values for the simulated stars and planets

*Interactive Data Language, ITT Corporation, http://www.ittvis.com/

Downloaded From: http://proceedings.spiedigitallibrary.org/ on 11/30/2016 Terms of Use: http://spiedigitallibrary.org/ss/termsofuse.aspx

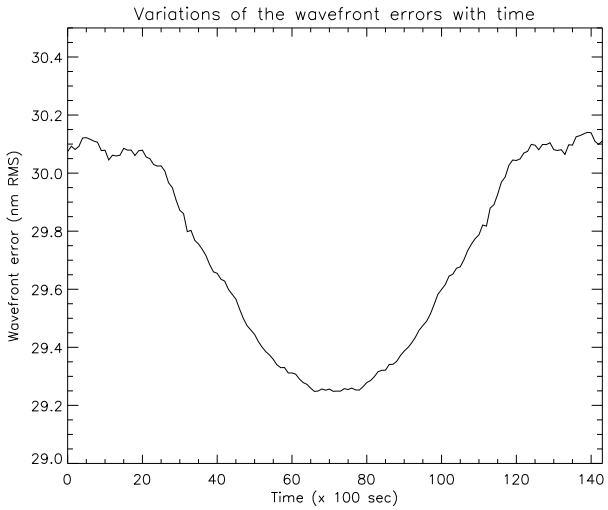

Figure 1. Evolution with time of the achromatic pre-coronagraph wavefront errors introduced in our simulation.

In this end-to-end model, the Fresnel propagation of the wavefront is not considered. However, the overall impact of Fresnel propagation has been evaluated in separate simulations (not detailed here) where pre-coronagraphic and post-coronagraphic propagation effects have been simulated. The main result is that while the region beyond AO cut-off (0.″8 in H band) is mostly dominated by the pre-coronagraphic propagation effects, resulting in a loss of up to a factor 2 in contrast, the inner region is affected by a mix of both effects, resulting in a loss of at most 1.5.

The complete simulated observation of 4 hours has been decomposed in individual images representing 100 s. At this timescale we assume that the fast-varying atmosphere residuals are averaged out and produce a smooth halo around the star, leaving only the correlated residuals with timescales longer than a few minutes. The 100-second timescale also allows to correctly sample the field rotation (120° in total for the 4 hours). During the course of the simulation, the seeing and wind speed have been varied on ranges typical for ESO-Paranal Observatory, respectively $0.85 \pm 0.''15$ and 14.2 ± 4.6 m s^{-1}. Optical aberrations have been varied according to the specifications of the optical elements of SPHERE. Figure 1 shows the variation of the pre-coronagraph achromatic wavefront errors as a function of time. The post-coronagraphic wavefront errors are dominated by a fixed amount of 50 nm RMS corresponding to IRDIS internal optics. The differential aberrations between the two DBI filters have been set to ∼7.5 nm RMS following the results obtained on IRDIS prototype filters.[11]

The diffractive code has been run to simulate data corresponding to the filter pairs Y2Y3, J2J3, H2H3 and K1K2 of IRDIS (Table 1). The output of this code is a series of normalized coronagraphic and non-coronagraphic images of the star at the two wavelengths of the filter pair. A second code was used to produce data cubes representing realistic planetary systems. For each star, 3 series of planets separated by 120° have been simulated at 0.″2, 0.″5, 1.″0, 1.″5 and 2.″0, taking into account the field rotation which is a function of the star elevation. Figure 2 shows a simulated coronagraphic image in filter H2 (left), and the simulated planets that have been

Table 1. List of IRDIS filter pairs.

Pair name	Filter 0		Filter 1	
	λ_0 (μm)	R_0	λ_1 (μm)	R_1
Y2Y3	1.020	20	1.073	20
J2J3	1.190	25	1.270	25
H2H3	1.587	30	1.667	30
H3H4	1.667	30	1.731	30
K1K2	2.100	20	2.244	20

Downloaded From: http://proceedings.spiedigitallibrary.org/ on 11/30/2016 Terms of Use: http://spiedigitallibrary.org/ss/termsofuse.aspx

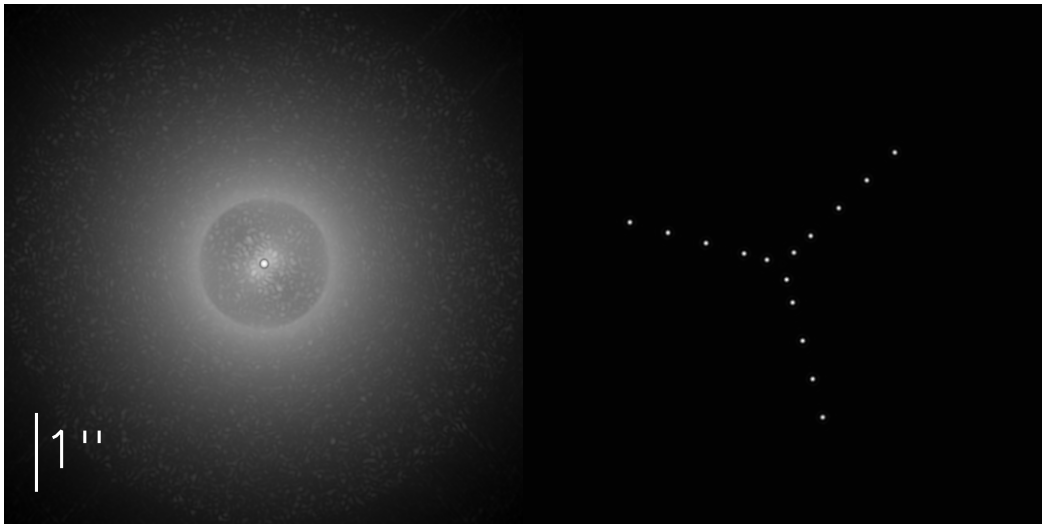

Figure 2. Coronagraphic image simulated for our test case in filter H2 of IRDIS (left) and the 3 series of planets at separations of 0.″2, 0.″5, 1.″0, 1.″5 and 2.″0 that have been introduced in all the simulated data cubes (right). The dark central area in the coronagraphic image corresponds to the area corrected by the extreme AO system.

introduced (right). Realistic photometry was calculated for the stars using standard Kurucz models[12,13] (spectral types regularly distributed from F0 to M0 at 10 pc), and the latest synthetic spectra for the planets, including the AMES-Dusty,[14] BT-Settl,[15] AMES-Cond,[16] and BSH.[17] The effective temperatures (T_{eff}) of the planets range from 350 K to 2500 K and the surface gravities (log g) from 2.5 to 6.0. The steps in the grids are of 100 K for T_{eff} and 0.5 for log g. For each filter pair we generated 66 data cubes with different combinations of star and planet to cover contrast values from $\sim 2 \times 10^{-7}$ to $\sim 10^{-2}$.

Finally, sky contribution has been added to match typical values for ESO-Paranal Observatory. Thermal background from the instrument was also included: the value is low in I, J and H bands (< 2 photon sec^{-1} pixel^{-1}), while it becomes significant in K band (60 to 220 photon sec^{-1} pixel^{-1}). A realistic amount of noise for the IRDIS detector was included in the images: photon noise, flat field noise (0.1%) and read-out noise (10 e$^-$/read). The final data cubes represent 4 h observations with IRDIS after standard cosmetic corrections and calibrations (dark, sky background and thermal background subtraction, flat field division, bad pixel correction and registration).

3. DATA ANALYSIS

3.1 Limitations in high-contrast imaging

High-contrast coronagraphic images are intrinsically limited by the speckle noise[18] induced by atmospheric phase residuals and instrumental quasi-static aberrations not corrected by the AO system. The quasi-static speckles are mainly caused by the instrumental aberrations that slowly change during a long exposure. On a timescale of a few seconds, the atmospheric residuals are averaged out forming a smooth halo around the star, over which the quasi-static speckles are superimposed because their coherence time is much longer.[19,20] To optimize AO performances and speckle rejection, observations can be performed in pupil-stabilized mode, leading to a very high stability of the PSF.

The speckle noise can be significantly reduced by subtracting a reference PSF to the science images in order to remove the static and quasi-static speckles. This reference PSF can be either obtained by observing a reference star in conditions similar to the ones of the science target, or by constructing a reference from the science data itself. The first solution is time-consuming and cannot exactly reproduce the speckle pattern between the target and the reference since the atmospheric conditions change, making impossible to perfectly match both PSFs. This is the reason why the second approach is generally favored.

Downloaded From: http://proceedings.spiedigitallibrary.org/ on 11/30/2016 Terms of Use: http://spiedigitallibrary.org/ss/termsofuse.aspx

Different techniques are available to obtain a reference PSF from the scientific observations. The first is to perform DBI,[21] where two images are acquired simultaneously at two close wavelengths located around expected sharp spectral features in the spectrum of cold planetary objects. Recent models predict the presence of large molecular absorption bands caused by H_2O, CH_4 and NH_3 at low T_{eff}. With carefully selected filters pairs, a contrast of several magnitudes on the planet flux between the two filters can be obtained, although some recent observations suggest that the presence of such molecular features should not be taken for granted, and would only appear at much lower T_{eff} than expected with current planetary atmosphere models.[22] Using these simultaneously acquired images, it is possible to perform Spectral Differential Imaging (SDI) by subtracting the 2 images obtained at λ_0 and λ_1.

Another technique is to use the fact that the field of view slowly rotates when observations are performed in pupil-stabilized mode. Angular Differential Imaging[23] (ADI) is performed by selecting for each image of interest, images taken before and after rotating the field of view by more than 1.5 λ/D. This operation is performed for all images in annuli of increasing radius. The global efficiency of ADI is mainly controlled by the rotation rate of the field of view, which depends on the star declination. At the latitude of ESO-Paranal observatory (-24° 3′ 38″) and for a star at declination $\delta = -45°$, the field rotation varies between 0.006 deg s^{-1} at an hour angle of ±2h and 0.011 deg s^{-1} at an hour angle of 0h. ADI can be further improved by using not only 2 images before and 2 images after each image of interest, but by finding the best linear combination of images separated by more than 1.5 λ/D than minimizes the residuals in the image of interest. This method is known as the Localy Optimized Combination of Images[24] (LOCI).

Finally, it is possible to combine SDI with ADI/LOCI in order to increase the speckle noise attenuation. SDI is first performed on short exposure images acquired simultaneously to remove the fast varying atmospheric residuals that have not been averaged out. ADI or LOCI is subsequently applied on this set of data to combine the images with different angular positions of the field of view.

3.2 Implementation of the different methods

SDI, ADI and LOCI have been tested on our simulated data for IRDIS in order to estimate the detection limits obtained with different data analysis methods. MOODS,[25,26] a data analysis method developed in the SPHERE consortium, has also been tested but only for the estimation of the simulated planet flux (see Sect. 4). Another data analysis method, ANDROMEDA,[27] has also been developed within the SPHERE consortium but has not been tested here. Future work will include a comparison of ANDROMEDA's results with the ones described in this work. For more details on ANDROMEDA, see Cornia et al. (this conference).

SDI implementation is straightforward: assuming that we use an extreme AO system, a perfect coronagraph, that aberrations are achromatic, and that the small phase approximation is valid, a coronagraphic star image at λ_i, denoted by $h_i^c(\alpha)$, scales spatially proportionally to λ_i, so that:

$$h_1^c(\frac{\lambda_1}{\lambda_0}\alpha) \propto h_0^c(\alpha) \tag{1}$$

Thus, assuming that the potential companion flux is negligible at wavelength λ_1, one can remove most of the star residuals in images at λ_0 by subtracting suitably rescaled simultaneous images at λ_1. Because SPHERE images are at least Shannon-sampled, this scaling can be done accurately using the discrete Fourier transform (DFT) – in practice the FFT. In a nutshell, our scaling method consists in zero-padding the image both in direct space and in Fourier space in order to obtain the zoom factor of our choice. The exact steps are detailed in Appendix A. The spatial rescaling of the image at λ_1 is a critical step to ensure that the speckle patterns match in both images.

ADI has been implemented following the thorough description given in Sect. 5.2 of Marois et al. (2006). The optimization has been performed in annuli with radii falling between our simulated planets: 0.″10, 0.″35, 0.″75, 1.″25, 1.″75 and 2.″25. For the LOCI, we used an implementation gently provided by D. Lafrenière and adapted by C. Thalmann to work on NaCo data and simulated data.

Downloaded From: http://proceedings.spiedigitallibrary.org/ on 11/30/2016 Terms of Use: http://spiedigitallibrary.org/ss/termsofuse.aspx

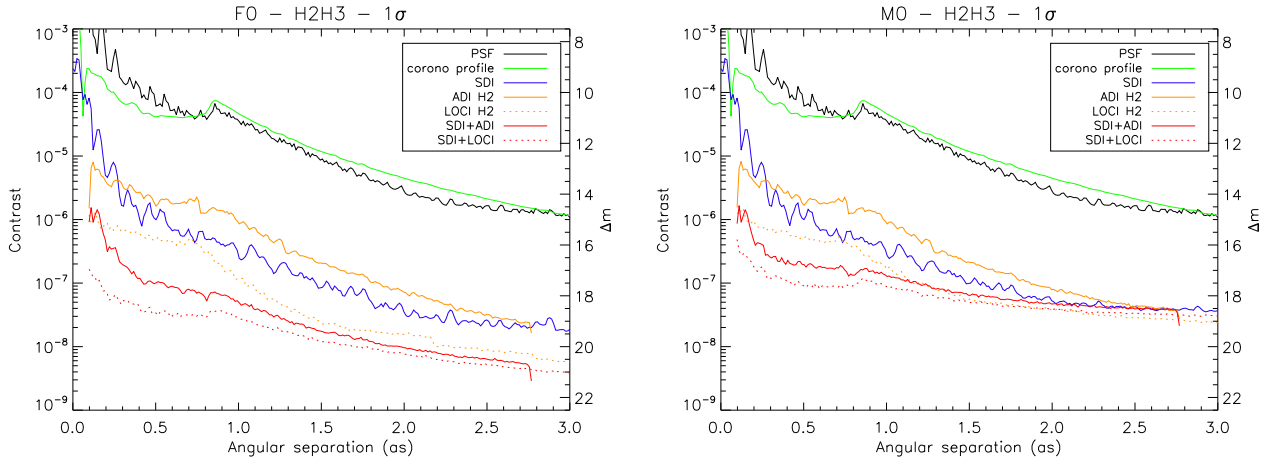

Figure 3. 1-σ noise level for a 4 hours observation in the H2H3 filter pair in high flux (F0 at 10 pc, top) and low flux (M0 at 10 pc, bottom) cases after applying different data analysis methods: SDI (blue plain line), ADI in filter H2 (orange plain line), LOCI in filter H2 (orange dotted line), SDI+ADI (red plain line) and SDI+LOCI (red dotted line). The level of the PSF (black plain line) and the coronagraphic profile (green plain line) are also shown for reference.

3.3 Speckle noise attenuation

Five different schemes of data analysis were tested on our simulated data sets:

1. SDI only,
2. ADI only (at λ_0 and λ_1 separately),
3. LOCI only (at λ_0 and λ_1 separately),
4. SDI+ADI,
5. SDI+LOCI.

Figure 3 presents the speckle noise level in H band after applying these schemes on simulated data for a 4-hours observation. Two different cases of star flux are considered, corresponding to different regimes of noise: a high flux case (F0 at 10 pc) and a low flux case (M0 at 10 pc). The PSF and coronagraphic profiles are calculated by the average of the PSF or coronagraphic images in annuli of increasing radius. The noise levels with all the data analysis methods are estimated from the standard deviation of the residuals in the same annuli. All curves are normalized to the maximum of the PSF without coronagraph.

We clearly see different levels of performances depending on the method that is used, the angular separation and the star flux regime. In high flux, where the performances are limited by the speckle noise and not by the photon and background noises, we see that SDI and ADI alone offer similar performances, with a small advantage for ADI at very small angular separations ($\lesssim 0\farcs2$), and for SDI at larger separations (0.5 to 1.0 mag between $0\farcs5$ and $2\farcs0$). These methods alone allow to reach contrasts of $\sim 4\times10^{-6}$ (13.5 mag) at $0\farcs2$ and $\sim 3\times10^{-8}$ (18.8 mag) at $3\farcs0$. When they are combined (SDI+ADI), the overall performance is clearly improved on the whole range of angular separations. The noise level is attenuated by 2 to 4 magnitudes depending on the separation, allowing to reach an ultimate contrast of $\sim 2\times10^{-7}$ (16.7 mag) at $0\farcs2$ and $\sim 5\times10^{-9}$ (20.8 mag) at $3\farcs0$. LOCI alone offers a significant improvement compared to ADI alone, with a gain of 1.5 to 2.5 magnitudes depending on the angular separation. At separations larger than $1\farcs5$, LOCI almost reaches the level of SDI+ADI, but SDI+ADI retains a clear advantage in the AO corrected region below $0\farcs85$. Finally, when combined with SDI, LOCI improves again the speckle noise attenuation, in particular at small angular separations, allowing to reach $\sim 5\times10^{-8}$ (18.3 mag) at $0\farcs2$.

Downloaded From: http://proceedings.spiedigitallibrary.org/ on 11/30/2016 Terms of Use: http://spiedigitallibrary.org/ss/termsofuse.aspx

In low star flux (M0 at 10 pc), the respective performances of the different methods are similar, but the higher level of photon noise, sky background noise and instrumental background noise clearly limit the contrast that can be reached at large angular separations. The effect is already visible at 0.″2, in particular for SDI+LOCI, which only reaches $\sim 2 \times 10^{-7}$ (16.7 mag), but it is extremely important at separations higher than 2.″0, where all methods reach a similar level of speckle noise attenuation. The effect is even worse in K band (not shown here) where the thermal emission of the sky and instrument is 10 to 15 times higher than in H band, limiting the contrast to $\sim 6 \times 10^{-7}$ (15.5 mag).

4. PHOTOMETRY

When a faint object is detected in the data, it needs to be characterized by measuring its intrinsic flux and comparing the measurements to planetary atmosphere models. In this section we investigate the photometric accuracy that can be reached after applying different data analysis methods on our simulated data. Due to the large amount of computing time required, only three data analysis methods have been considered: ADI, SDI+ADI and MOODS. MOODS is a method based on maximum likelihood and developed within the SPHERE consortium. It will be implemented (among others) within the instrument data reduction pipeline. In the case of MOODS, 4 contrast values close to 10^{-6}, 10^{-5}, 10^{-4} and 10^{-3} have been tested to obtain a general idea of the accuracy. Moreover, when both spectral information from filters H2 and H3 are used, MOODS gives as the output both flux values in H2 and H3 filters instead of the differential flux (H2-H3), as SDI does.

4.1 Planet flux estimation

For ADI and SDI+ADI, the flux of all planets detected at more than 5-σ was estimated using aperture photometry in a aperture of diameter $2.44\lambda/D$. The aperture was calculated to take into account the effect of using a round aperture on square pixels. The measured signal was converted to a flux in phot s^{-1} m^{-2} with the formula:

$$f_i = \frac{S_i}{E_e \; S_{\mathrm{Tel}} \; T_r \; t_i}, \tag{2}$$

where S_i is the measured signal on image i, E_e is the encircled energy in the aperture, S_{Tel} is the telescope collecting surface, T_r is the transmission of the atmosphere, telescope and instrument, and t_i is the exposure time for image i (100 s in our case). We have considered that the E_e in the aperture is known. Its value mostly varies with seeing conditions because the AO correction will concentrate more energy in the PSF core when seeing improves. Moreover we have corrected the measured signal from the PSF smearing caused by the rotation of the field of view during the simulated exposure time of 100 s. In practice, exposure time of single images will be of the order of a few seconds, greatly reducing the impact of smearing.

For MOODS, the planet flux in both filters of a pair is one of the output of the method. It also provides an uncertainty on these estimations of flux. It does not require the use of any particular aperture. For more details on the principle and implementation of MOODS, see Smith et al. (2008). The statistical properties of the MOODS estimation and detection scheme are analyzed in Smith et al. (2009).

4.2 Comparison of ADI, SDI+ADI and MOODS

Figure 4 presents the error on the planet flux estimation with ADI, SDI+ADI, and MOODS, as a function of contrast and angular separation in the filter pair H2H3 of IRDIS. We see that for the three methods and for all angular separations the trends are identical: the error remains low ($\lesssim 0.05$ mag) down to a given value of contrast, and for lower contrast values the error increases exponentially. As can be expected, the contrast value at which the error starts to increase is higher at small angular separations because of the more important level of speckle noise close to the star. The error bars in ADI and SDI+ADI correspond to the flux estimations of the three simulated planets at the given separations (see Fig. 2). For MOODS, the estimation was only made on 1 planet at each separation. One of the main advantages of statistical methods like MOODS is that they allow an estimation of the error on the flux from the science data itself. However, since the data are actually described by a statistical model more complex than the underlying model used to derive all methods (Gaussian model), the estimation of the uncertainty only gives the magnitude order of the uncertainty.

Downloaded From: http://proceedings.spiedigitallibrary.org/ on 11/30/2016 Terms of Use: http://spiedigitallibrary.org/ss/termsofuse.aspx

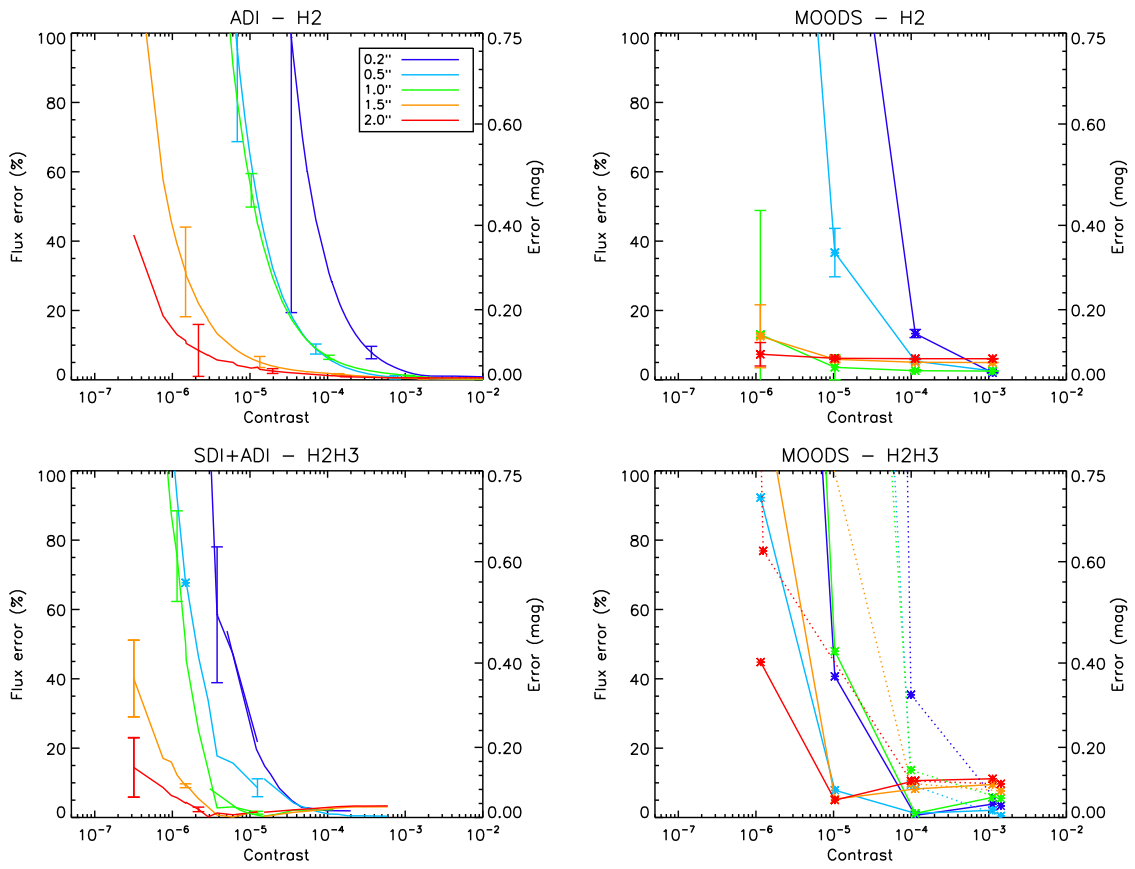

Figure 4. Planet flux estimation error as a function of contrast in filter pair H2H3 of IRDIS using ADI in H2 (top left), SDI+ADI in H2H3 (bottom left), MOODS in H2 (top right) and MOODS in H2H3 (bottom right). MOODS with both spectral information in filters H2 and H3 gives an estimation of the flux H2 and H3 independently (H3 error is plotted in dotted line).

With a photometric precision better than 0.2 mag, current evolutionary models should allow a determination of the planet T_{eff} with a precision better than 50 K. With ADI (top left plot) we see that such a precision can be reached down to a contrast value of $\sim 2 \times 10^{-4}$ (9.2 mag) at very small angular separation, and down to $\sim 6 \times 10^{-7}$ (15.6 mag) at 2.″0. The error bars are much wider at small angular separations where the speckle residuals are more important. If we compare these results to MOODS in filter H2 alone (top right plot), we see that the precision is similar for separations lower or equal to 0.″5, but that MOODS seems to offer a better estimation of the flux at separations larger or equal to 1.″0. When both spectral information are used with MOODS (bottom right plot) to obtain a joint estimation of H2 and H3, the error at 0.″2 and 0.″5 are clearly improved in H2 reaching a precision of 0.2 mag respectively at contrasts of $\sim 3 \times 10^{-5}$ (11.3 mag) and $\sim 7 \times 10^{-6}$ (12.9 mag). However, the flux estimation becomes worse than with ADI alone at larger angular separations. We also see an error that seems to increase when the contrast is more favorable at such separations. In H3, the contrast is lower because H3 lies on an absorption band of the simulated planetary atmosphere models, but we see that the estimation precision is comparable to H2 alone. These results are difficult to quantify and to analyze precisely given the very small number of measurement points for MOODS. A more extended analysis is required to draw definitive conclusions.

SDI+ADI uses both images obtained with filters H2 and H3 to provide a differential flux measurement. Similarly to the speckle noise attenuation, combining spectral and angular methods significantly improves the results at all angular separations. In particular, at 0.″2 a precision of 0.2 mag is reached at a contrast value of $\sim 10^{-5}$ (12.5 mag), improving by a factor 20 compared to ADI alone. The improvement factor is less significant

Downloaded From: http://proceedings.spiedigitallibrary.org/ on 11/30/2016 Terms of Use: http://spiedigitallibrary.org/ss/termsofuse.aspx

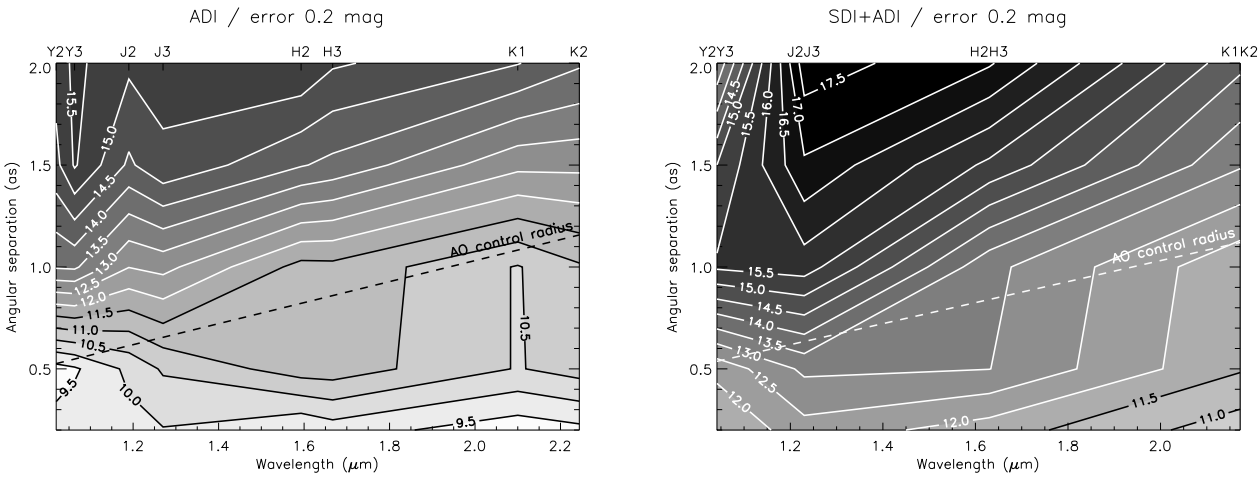

Figure 5. Magnitude difference between the star and the planet for which the photometric precision is better than 0.2 mag, as a function of wavelength and angular separation using ADI (left) and SDI+ADI (right) data analysis methods. The oblique dashed-line shows the AO control radius limit (from Vigan et al. 2010).

at larger angular separations but is in any case larger than 5. Moreover, flux estimation with SDI+ADI is more sensitive to small errors such as positioning of the aperture for photometry, because it uses a double aperture to cover both PSFs of the planet at λ_0 and λ_1.

The photometric precision in ADI and SDI+ADI has also been studied in other IRDIS filter pairs, namely Y2Y3, J2J3, and K1K2. Figure 5 (taken from Vigan et al. (2010)[28]) illustrates the photometric performance as a function of wavelength and angular separation from the star. The contours indicate the contrast value between the star and planet below which the photometric precision is better than 0.2 mag. Two major effects can be seen on this plots:

1. the photometric performance clearly depends on wavelength,
2. there are two different regimes depending on the position compared to the AO control radius.

The first effect is directly related to the PSF chromaticity, while the second is related to the AO correction inside the corrected region. Inside that region we see a stabilization of the performance in ADI: 0.2 mag photometric precision is reached for contrasts of $\sim 10^{-4}$ to $\sim 4 \times 10^{-5}$ (10 to 11 mag), while at larger separations the performance increases linearly with wavelength. In SDI+ADI these results are less visible because the effects related to chromaticity have been attenuated by the use of SDI before ADI. We see that with ADI, a photometric precision of 0.2 mag can be reached down to a contrast of $\sim 10^{-4}$ (10 mag) at very close separation for all wavelengths. At larger separation the same performance is reached for contrasts of $\sim 2.5 \times 10^{-6}$ to $\sim 10^{-6}$ (14 to 15 mag). Combining SDI+ADI increases these values by 1.5 to 2.5 mag at all wavelengths and separations, except in Y band where the aperture for photometry is very small (4 pixels in diameter) and for which the influence of field rotation and planet PSF smearing is important, and thus difficult to correct.

5. CONCLUSION

In the context of SPHERE we have performed a detailed simulation of a 4 hours observing sequence with IRDIS, the dual-band imager of SPHERE. In this simulation, a large number of effects with their temporal evolution have been taken into account: seeing, wind speed, AO correction, optics rotation, ADC chromatic residuals, pointing errors, field of view rotation. Various detector effects have also been included in the simulation. Planets at angular separations of $0''.2$, $0''.5$, $1''.0$, $1''.5$ and $2''.0$ have been simulated and photometry was calculated with a large number of different planets and stars in order to cover contrast differences between $\sim 2 \times 10^{-7}$ and $\sim 10^{-2}$.

Downloaded From: http://proceedings.spiedigitallibrary.org/ on 11/30/2016 Terms of Use: http://spiedigitallibrary.org/ss/termsofuse.aspx

Using this unique set of data, we have tested various data analysis methods to estimate the detection limits: Spectral Differential Imaging (SDI), Angular Differential Imaging (ADI), SDI+ADI, Localy Optimized Combination of Images (LOCI), and SDI+LOCI. We showed that the combination of SDI and LOCI allows to reach contrasts of $\sim 2 \times 10^{-7}$ (16.7 mag) at a separation of $0''.2$ and $\sim 5 \times 10^{-9}$ (20.8 mag) at $3''.0$.

For the characterization of the detected objects, we have studied the photometric error obtained after using ADI, SDI+ADI, and MOving Object Detection for Sphere (MOODS). We showed that ADI and MOODS in the H2 filter offer similar photometric performances, in particular at close angular separations, and that MOODS with both spectral information in filters H2 and H3 significantly improves the photometric performance at small angular separations. However, it seems that the performance degrades at larger angular separations with the latter. New simulations are required in order to investigate this effect. Combining SDI+ADI to obtain a differential flux measurement also greatly improves the photometric performance compared to ADI alone in H band. Finally, we showed that the photometric performance in ADI and SDI+ADI has a strong dependance on wavelength due to the PSF chromaticity, and on the position compared to the AO control radius limit. Note that a detailed analysis of the impact of these results on future exoplanets characterization with IRDIS DBI mode can be found in Vigan et al. (2010).

ACKNOWLEDGMENTS

SPHERE is an instrument designed and built by a consortium consisting of LAOG, MPIA, LAM, LESIA, Laboratoire Fizeau, INAF, Observatoire de Genève, ETH, NOVA, ONERA and ASTRON in collaboration with ESO.

APPENDIX A. SPATIAL SCALING ALGORITHM DETAILS

For conciseness we consider one-dimensional signals, and the results generalize readily to two dimensions. Given N samples of a signal i sampled with a pitch p_α, the quantity $\tilde{i}(k.p_\nu)$ given by:

$$\tilde{i}(k.p_\nu) = \sum_{l=0}^{N-1} i(l.p_\alpha)\, e^{2j\pi\, l p_\alpha\, k p_\nu}, \tag{3}$$

is the DFT of i at frequency $k.p_\nu$, where p_ν is the pitch in Fourier space. Because of the use of the FFT, the pitch in Fourier and direct spaces are related by

$$p_\alpha p_\nu = 1/N, \tag{4}$$

which means that the support Np_α is the inverse of the Fourier pitch.

If we modify the number of pixels in direct space by adding on each side of the table some null pixels *before* performing the FFT, Eq. (4) becomes $p_\alpha p_{\nu'} = 1/N'$, where N' is the new signal size after zero-padding in direct space, and $p_{\nu'}$ the new pitch in Fourier space.

If we proceed similarly in Fourier space by adding null pixels after performing the FFT, we finally obtain for the new spatial sampling in direct space after an inverse FFT:

$$p_{\alpha"} = (N'/N")\, p_\alpha, \tag{5}$$

where $N"$ is the new signal size after zero-padding in Fourier space. We have thus zoomed the image by a factor $z = (N"/N')$. Note that if we only zero-pad the image in Fourier space, as it is often done, then $N' = N$, which severely constrains the zooming factor: $z = N"/N$.

In order to resample the coronagraphic star image at λ_1 according to Eq. (1), we need to satisfy the following equation:

$$\frac{N'}{N"} = \frac{\lambda_1}{\lambda_0}. \tag{6}$$

Having two degrees of freedom N' and $N"$ allows us, in practice, to satisfy this equality with a good precision (10^{-4} or so) for reasonable values of N' and $N"$ for all wavelengths of the IRDIS instrument.

Downloaded From: http://proceedings.spiedigitallibrary.org/ on 11/30/2016 Terms of Use: http://spiedigitallibrary.org/ss/termsofuse.aspx

REFERENCES

[1] Macintosh, B., Graham, J., and Palmer, D. et al., "The Gemini Planet Imager," in [*SPIE Conference Series*], **6272** (July 2006).

[2] Hodapp, K. W., Suzuki, R., and Tamura, M. et al., "HiCIAO: the Subaru Telescope's new high-contrast coronographic imager for adaptive optics," in [*SPIE Conference Series*], **7014** (Aug. 2008).

[3] Fusco, T., Petit, C., and Rousset, G. et al., "Design of the extreme AO system for SPHERE, the planet finder instrument of the VLT," in [*SPIE Conference Series*], **6272** (July 2006).

[4] Rouan, D., Riaud, P., Boccaletti, A., Clénet, Y., and Labeyrie, A., "The Four-Quadrant Phase-Mask Coronagraph. I. Principle," *PASP* **112**, 1479–1486 (Nov. 2000).

[5] Mawet, D., Riaud, P., Baudrand, J., Baudoz, P., Boccaletti, A., Dupuis, O., and Rouan, D., "The four-quadrant phase-mask coronagraph: white light laboratory results with an achromatic device," *A&A* **448**, 801–808 (Mar. 2006).

[6] Soummer, R., "Apodized Pupil Lyot Coronagraphs for Arbitrary Telescope Apertures," *ApJ Letter* **618**, L161–L164 (Jan. 2005).

[7] Antichi, J., Dohlen, K., and Gratton, R. et al., "BIGRE: A Low Cross-Talk Integral Field Unit Tailored for Extrasolar Planets Imaging Spectroscopy," *ApJ* **695**, 1042–1057 (Apr. 2009).

[8] Dohlen, K., Langlois, M., and Saisse, M. et al., "The infra-red dual imaging and spectrograph for SPHERE: design and performance," in [*SPIE Conference Series*], **7014** (Aug. 2008).

[9] Carbillet, M., Verinaud, C., and Guarracino, M. et al., "CAOS: a numerical simulation tool for astronomical adaptive optics (and beyond)," in [*SPIE Conference Series*], Bonaccini Calia, D., Ellerbroek, B. L., and Ragazzoni, R., eds., **5490**, 637–648 (Oct. 2004).

[10] Carbillet, M., Boccaletti, A., and Thalmann, C. et al., "The Software Package SPHERE: a CAOS-based numerical tool for end-to-end simulations of SPHERE/VLT," in [*SPIE Conference Series*], **7015** (July 2008).

[11] Dohlen, K., Saisse, M., and Origne, A. et al., "Prototyping of differential optics for the SPHERE IRDIS dual imaging planet finder camera," in [*SPIE Conference Series*], **7018** (July 2008).

[12] Kurucz, R. L., "Model atmospheres for G, F, A, B, and O stars," *ApJ* **40**, 1–340 (May 1979).

[13] Castelli, F. and Kurucz, R. L., "New Grids of ATLAS9 Model Atmospheres," in [*Modelling of Stellar Atmospheres*], Piskunov, N., Weiss, W. W., and Gray, D. F., eds., *IAU Symposium* **210**, 20P–+ (2003).

[14] Allard, F., Hauschildt, P. H., Alexander, D. R., Tamanai, A., and Schweitzer, A., "The Limiting Effects of Dust in Brown Dwarf Model Atmospheres," *ApJ* **556**, 357–372 (July 2001).

[15] Allard, F., Allard, N. F., Homeier, D., Kielkopf, J., McCaughrean, M. J., and Spiegelman, F., "K-H_2 quasi-molecular absorption detected in the T-dwarf \varepsilon Indi Ba," *A&A* **474**, L21–L24 (Nov. 2007).

[16] Allard, F., Guillot, T., Ludwig, H.-G., Hauschildt, P. H., Schweitzer, A., Alexander, D. R., and Ferguson, J. W., "Model Atmospheres and Spectra: The Role of Dust," in [*Brown Dwarfs*], Martín, E., ed., *IAU Symposium* **211**, 325–+ (June 2003).

[17] Burrows, A., Sudarsky, D., and Hubeny, I., "L and T Dwarf Models and the L to T Transition," *ApJ* **640**, 1063–1077 (Apr. 2006).

[18] Soummer, R., Ferrari, A., Aime, C., and Jolissaint, L., "Speckle Noise and Dynamic Range in Coronagraphic Images," *ApJ* **669**, 642–656 (Nov. 2007).

[19] Macintosh, B., Poyneer, L., Sivaramakrishnan, A., and Marois, C., "Speckle lifetimes in high-contrast adaptive optics," in [*SPIE Conference Series*], Tyson, R. K. and Lloyd-Hart, M., eds., **5903**, 170–177 (Aug. 2005).

[20] Hinkley, S., Oppenheimer, B. R., and Soummer, R. et al., "Temporal Evolution of Coronagraphic Dynamic Range and Constraints on Companions to Vega," *ApJ* **654**, 633–640 (Jan. 2007).

[21] Racine, R., Walker, G. A. H., Nadeau, D., Doyon, R., and Marois, C., "Speckle Noise and the Detection of Faint Companions," *PASP* **111**, 587–594 (May 1999).

[22] Fortney, J. J., Marley, M. S., Saumon, D., and Lodders, K., "Synthetic Spectra and Colors of Young Giant Planet Atmospheres: Effects of Initial Conditions and Atmospheric Metallicity," *ApJ* **683**, 1104–1116 (Aug. 2008).

Downloaded From: http://proceedings.spiedigitallibrary.org/ on 11/30/2016 Terms of Use: http://spiedigitallibrary.org/ss/termsofuse.aspx

[23] Marois, C., Lafrenière, D., Doyon, R., Macintosh, B., and Nadeau, D., "Angular Differential Imaging: A Powerful High-Contrast Imaging Technique," *ApJ* **641**, 556–564 (Apr. 2006).

[24] Lafrenière, D., Marois, C., Doyon, R., Nadeau, D., and Artigau, É., "A New Algorithm for Point-Spread Function Subtraction in High-Contrast Imaging: A Demonstration with Angular Differential Imaging," *ApJ* **660**, 770–780 (May 2007).

[25] Smith, I., Carbillet, M., Ferrari, A., Mouillet, D., Boccaletti, A., and Dohlen, K., "Simulation of moving exoplanets detection using the VLT instrument SPHERE/IRDIS," in [*Society of Photo-Optical Instrumentation Engineers (SPIE) Conference Series*], *Society of Photo-Optical Instrumentation Engineers (SPIE) Conference Series* **7015** (July 2008).

[26] Smith, I., Ferrari, A., and Carbillet, M., "Detection of a Moving Source in Speckle Noise. Application to Exoplanet Detection," *IEEE Transactions on Signal Processing* **57**, 904–915 (Mar. 2009).

[27] Mugnier, L. M., Cornia, A., Sauvage, J.-F., Rousset, G., Fusco, T., and Védrenne, N., "Optimal method for exoplanet detection by angular differential imaging," *J. Opt. Soc. Am. A* **26**, 1326–1334 (June 2009).

[28] Vigan, A., Moutou, C., Langlois, M., Allard, F., Boccaletti, A., Carbillet, M., Mouillet, D., and Smith, I., "Photometric exoplanet characterization with angular and spectral differential imaging," *ArXiv e-prints* (Apr. 2010).

Downloaded From: http://proceedings.spiedigitallibrary.org/ on 11/30/2016 Terms of Use: http://spiedigitallibrary.org/ss/termsofuse.aspx